Title

Metabolic Imaging of Patients with Prostate Cancer Using Hyperpolarized [1-13C]Pyruvate

Journal

Science Translational Medicine, 5(198)

ISSN

1946-6234

Authors

Nelson, Sarah J

Kurhanewicz, John

Vigneron, Daniel B

et al.

Publication Date

2013-08-14

DOI

10.1126/scitranslmed.3006070

Peer reviewed

Published in final edited form as:
Sci Transl Med. 2013 August 14; 5(198): 198ra108. doi:10.1126/scitranslmed.3006070.

Metabolic Imaging of Patients with Prostate Cancer Using Hyperpolarized [1-^{13}C]Pyruvate

Sarah J. Nelson[1,2,*], **John Kurhanewicz**[1], **Daniel B. Vigneron**[1,2], **Peder E. Z. Larson**[1], **Andrea L. Harzstark**[3], **Marcus Ferrone**[4], **Mark van Criekinge**[1], **Jose W. Chang**[4], **Robert Bok**[1], **Ilwoo Park**[1], **Galen Reed**[1], **Lucas Carvajal**[1], **Eric J. Small**[3], **Pamela Munster**[3], **Vivian K. Weinberg**[5], **Jan Henrik Ardenkjaer-Larsen**[6], **Albert P. Chen**[6], **Ralph E. Hurd**[6], **Liv-Ingrid Odegardstuen**[6], **Fraser J. Robb**[7], **James Tropp**[6], and **Jonathan A. Murray**[6]

[1]Surbeck Laboratory of Advanced Imaging, Department of Radiology and Biomedical Imaging, University of California, San Francisco, San Francisco, CA 94158, USA

[2]Department of Bioengineering and Therapeutic Sciences, University of California, San Francisco, San Francisco, CA 94158, USA

[3]Department of Medicine, University of California, San Francisco, San Francisco, CA 94143, USA

[4]Department of Clinical Pharmacy, University of California, San Francisco, San Francisco, CA 94143, USA

[5]Department of Biostatistics, University of California, San Francisco, San Francisco, CA 94143, USA

[6]General Electric Healthcare, Waukesha, WI 53188, USA

[7]USA Instruments Inc., Aurora, OH 44202, USA

Abstract

This first-in-man imaging study evaluated the safety and feasibility of hyperpolarized [1-^{13}C]pyruvate as an agent for noninvasively characterizing alterations in tumor metabolism for patients with prostate cancer. Imaging living systems with hyperpolarized agents can result in

*Corresponding author. sarah.nelson@ucsf.edu.

Author contributions: S.J.N., D.B.V., and J.K. planned the project and coordinated and oversaw the patient studies. P.E.Z.L. developed pulse sequences and acquired and processed the ^{13}C data. A.L.H. was the oncologist who designed the patient studies, obtained the IND, and cared for patients. M.F. was the pharmacist responsible for all aspects of the compounding process. M.v.C. was responsible for engineering design and polarizer function. J.W.C. was responsible for the clean room, polarizations, and dissolutions. R.B. monitored patients. I.P. was responsible for postprocessing and data analysis. G.R. acquired preclinical and patient data. L.C. was responsible for specialized hardware and radio frequency coils. E.J.S. and P.M. participated in designing the patient studies. V.K.W. provided statistical input for study design and interpretation of the results. J.H.A.-L. was responsible for the polarizer design and for providing advice on protocol development. A.P.C. and R.E.H. contributed to engineering development. L.-I.O. coordinated the provision of sterile components and the material used to produce the imaging agent. F.J.R. provided input on radio frequency coil design and system integration. J.T. designed, constructed, and tested the radio frequency coils. J.A.M. developed the study concept and coordinated the academic-industry partnership that made the clinical trial possible.

Competing interests: Some of the MRI acquisition methods that were used have been patented (#7,795,868). The authors have no other competing interests to declare.

Data and materials availability: Information about the pulse sequence design and data processing methods is available through the NIH-supported Hyperpolarized MRI Technology Resource Center at UCSF (www.radiology.ucsf.edu/research/labs/hyperpolarized-mri-tech). The endorectal coil is patented by General Electric and cannot be made and sold for profit except under license.

more than 10,000-fold enhancement in signal relative to conventional magnetic resonance (MR) imaging. When combined with the rapid acquisition of in vivo ^{13}C MR data, it is possible to evaluate the distribution of agents such as [1-^{13}C]pyruvate and its metabolic products lactate, alanine, and bicarbonate in a matter of seconds. Preclinical studies in cancer models have detected elevated levels of hyperpolarized [1-^{13}C]lactate in tumor, with the ratio of [1-^{13}C]lactate/[1-^{13}C]pyruvate being increased in high-grade tumors and decreased after successful treatment. Translation of this technology into humans was achieved by modifying the instrument that generates the hyperpolarized agent, constructing specialized radio frequency coils to detect ^{13}C nuclei, and developing new pulse sequences to efficiently capture the signal. The study population comprised patients with biopsy-proven prostate cancer, with 31 subjects being injected with hyperpolarized [1-^{13}C]pyruvate. The median time to deliver the agent was 66 s, and uptake was observed about 20 s after injection. No dose-limiting toxicities were observed, and the highest dose (0.43 ml/kg of 230 mM agent) gave the best signal-to-noise ratio for hyperpolarized [1-^{13}C]pyruvate. The results were extremely promising in not only confirming the safety of the agent but also showing elevated [1-^{13}C]lactate/[1-^{13}C]pyruvate in regions of biopsy-proven cancer. These findings will be valuable for noninvasive cancer diagnosis and treatment monitoring in future clinical trials.

Introduction

Prostate cancer is one of the most common cancers, with more than 200,000 new cases being reported annually in the United States (1). Owing to increased screening using serum prostate-specific antigen (PSA) and extended-template transrectal ultrasound (TRUS)–guided biopsies, patients with prostate cancer are being identified at an earlier and potentially more treatable stage (2). Once detected, the decision on how to manage prostate cancer poses a dilemma because there is a tremendous range in biologic diversity. They are treated with a broad spectrum of approaches from “active surveillance” to more aggressive surgical, radiation-based, and other focal therapies (3, 4). Such therapies have trade-offs because, no matter how well they are delivered, there can be changes in health-related quality of life (5). In practice, many prostate cancers follow an indolent course that would not threaten the duration or quality of lives for the affected men, but the natural history of individual tumors is difficult to predict using currently available prognostic data (6, 7). Conversely, between 22 and 35% of men presenting with clinically advanced prostate cancer, who are treated with what was thought to be definitive radiation or surgery, suffer a posttreatment biochemical recurrence (8). The ability to predict outcome for individual patients and thereby select the most appropriate treatment is a critically important, but so far unmet, clinical need.

Although noninvasive imaging is used to assess prostate cancer, conventional techniques have limited value for assessing prognosis, and there is no widely accepted modality that provides information about aggressiveness and response to therapy (9). Proton magnetic resonance spectroscopic imaging (^{1}H MRSI) has been applied to assess the metabolic properties of localized prostate cancer and, although it has shown clear advantages over anatomic imaging alone (10), is limited by its relatively low spatial resolution and acquisition time, which is in the range of 10 to 20 min (11). ^{18}F-Fluorodeoxyglucose

positron emission tomography provides information about increased glucose uptake and phosphorylation, but has been shown to inadequately evaluate the presence and aggressiveness of prostate cancer because of both its relatively low uptake and collection in the bladder (12).

Hyperpolarized ^{13}C MRI is a new molecular imaging technique with an unprecedented gain in signal intensity of 10,000- to 100,000-fold (13) that can be used to monitor uptake and metabolism of endogenous biomolecules (14, 15). The magnitude of the increase in sensitivity depends on the degree of polarization that is achieved, the T_1 relaxation time of the ^{13}C agent, the delivery time, and the MR methods applied. Hyperpolarized agents are generated by mixing ^{13}C-labeled compounds with an electron paramagnetic agent (EPA), placing them in a 3.35-T magnetic field, cooling to ~1 K, and using microwaves to transfer polarization from the electron spin of the EPA to the ^{13}C nuclei of the biomolecule (13). Once the polarization has reached the required level, the sample is rapidly dissolved with hot, sterile water and neutralized to physiological pH, temperature, and osmolarity. Intravenous injection of the hyperpolarized solution and observation using ^{13}C MR allow its delivery and metabolic products to be monitored (15). The data must be obtained as rapidly as possible after dissolution because the enhancement decays at a rate determined by the T_1 relaxation time of the agent, which is about 60 s for [1-^{13}C]pyruvate at 3 T. Translation of hyperpolarized technology into human subjects has been challenging because it requires specialized instrumentation to prepare the agent in a sterile environment, filter out the EPA, perform quality control (QC), and rapidly deliver samples to the patient.

The acquisition of ^{13}C data can be achieved using commercially available MR scanners in conjunction with specialized pulse sequences (16) and radio frequency coils designed to transmit and receive at the appropriate frequency. Increased signal from hyperpolarized [1-^{13}C]lactate has been observed in preclinical models of prostate cancer relative to normal tissues, owing to both increased uptake of [1-^{13}C]pyruvate via monocarboxylate transporters 1 and 4 (MCT1 and MCT4) and increased expression of LDH-A and activity of lactate dehydrogenase (LDH) (17). Levels of hyperpolarized [1-^{13}C]lactate and the flux of [1-^{13}C]pyruvate to [1-^{13}C]lactate increase with cancer progression (pathologic grade) (18) and reduce after therapy (19, 20).

The primary goal of this first-in-human study was to demonstrate the safety and feasibility of hyperpolarized [1-^{13}C]pyruvate injections in men with prostate cancer. After establishing the maximum of three dose levels that could be safely delivered, the secondary aims were to evaluate the kinetics of delivery to the prostate and assess differences in [1-^{13}C]lactate/[1-^{13}C]pyruvate for regions of cancer versus other tissues. Successfully demonstrating that the technology can be applied to humans provides the opportunity to use it for detecting and staging cancer, as well as detecting tumor progression and monitoring response to therapy.

Results

Study design: Doses delivered and data acquisition

There were 31 patients with untreated, biopsy-proven localized prostate cancer who received an injection of hyperpolarized [1-^{13}C]pyruvate. Their median age was 63 years (range, 45 to

75), median PSA was 5.9 ng/ml (range, 1.88 to 20.2), and median LDH was 141 IU/liter (range, 109 to 261). Twenty-three of them had a diagnosis of Gleason grade 6 tumor, 6 had Gleason grade 7 tumor, and 2 had Gleason grade 8 tumor. The initial (phase 1) component of the study used a standard dose escalation design (Table 1), with six subjects being evaluated at each of three ascending doses. Dose levels were chosen on the basis of the range that had been shown to be safe in previous studies that did not include imaging but did inject nonlabeled pyruvate at the same concentrations, pH, and delivery rate (Supplementary Methods). At each dose, three patients were scanned with a dynamic ^{13}C sequence that provided localization to one-dimensional (1D) slices through the prostate, and three patients were scanned with a ^{13}C sequence that provided 2D or 3D spatial localization at a single time point. An additional 13 subjects were evaluated at the highest dose level in phase 2 with a mixture of dynamic and single–time point ^{13}C MR sequences. The specialized ^{13}C volume transmit coil and dual $^{1}H/^{13}C$ endorectal coil that were designed and built for this study are shown in Fig. 1, A to C. These functioned well and allowed ^{1}H images and ^{13}C spectral data to be acquired from all subjects.

Hyperpolarized pyruvate polarization and delivery

For the 31 samples injected into patients, the average polarization was 17.8% (range, 15.9 to 21.1), pH was 7.6 (range, 7.3 to 8.0), temperature was 32.4°C (range, 28.8 to 36.4), and volume was 51.9 ml (range, 31.9 to 53.5). QC criteria were defined as follows: polarization to be not less than 15%, pH in the range of 6.7 to 8.0, sample temperature in the range of 25° to 37°C, and residual EPA concentration no higher than 3.0 μg. The mean times for getting the sample to the patient are seen schematically in Fig. 1D: the dissolution took an average of 17.8 s (range, 5 to 30), the QC process 13.1 s (range, 10 to 19), delivery through the hatch into the scan room 21.8 s (range, 11 to 30), and injection 14.9 s (range, 6 to 28). Overall, this gave an average of 67.6 s (range, 43 to 88) to deliver the agent to the subject. The parameters for individual patients are given in table S1. The mean injection volumes for the patients studied at each dose were 11.8 ml (range, 10 to 14), 26.8 ml (range, 22 to 33), and 34.5 ml (range, 29 to 46), with mean injection times of 8.5 s (range, 6 to 10), 14.8 s (range, 10 to 27), and 12.5 s (range, 1 to 28), respectively. Variation in injection times reflected differences in the volume delivered, as well as in the time for drawing the material from the drug product vessel into a syringe and performing the manual injection.

Patient toxicities

Vital signs were monitored before and immediately after the imaging examination, with subsequent telephone follow-ups over a period of 7 days to check for evidence of adverse events. In phase 1 of the study, there were a total of 10 adverse events in eight patients (table S2). These were all considered mild events and were classified as grade 1 by Common Terminology Criteria for Adverse Events (CTCAE) v4.0.criteria (21). The highest dose of [1-^{13}C]pyruvate (0.43 ml/kg) was selected for further study on the basis of the higher signal-to-noise ratio (SNR) of hyperpolarized [1-^{13}C]pyruvate that was observed. In phase 2, there were an additional 10 events observed in five patients, but, again, none of them were considered to be dose-limiting toxicities (DLTs). The single episode of dizziness that was seen in one patient during phase 2 was attributed to extra dosing of atenolol, which was used by the subject to reduce anxiety rather than the hyperpolarized agent. There was one episode

of grade 2 diarrhea reported in the phase 2 component, which was attributed to an enema that the patient received.

1D dynamic MRSI

The purpose of the 1D spatially localized dynamic data was to establish the time course of delivery of the agent. The acquisition provided spectra from an axial slab that covered the prostate and surrounding tissues and applied echo planar encoding from slices in the right-left direction at a 3-s time resolution. These dynamic data demonstrated reproducible delivery of hyperpolarized [1-^{13}C]pyruvate to the prostate and its conversion to hyperpolarized [1-^{13}C]lactate. Figure 2A shows a representative scan from a patient with PSA of 12.2 ng/ml, who had a small volume of biopsy-proven prostate cancer (Gleason grade 4 + 3) in the left midgland and received the lowest dose of 0.14 ml/kg. Representative ^{13}C spectra from the same patient taken from a slice including the tumor 36 s after injection demonstrated peaks corresponding to [1-^{13}C]pyruvate [173 parts per million (ppm)] and [1-^{13}C]lactate (185 ppm) (Fig. 2B). Spectra from the contralateral side of the prostate demonstrated only [1-^{13}C]pyruvate. A plot of spectral peak heights from the slice overlapping the tumor is shown in Fig. 2C and from the slice on the contralateral side of the gland in Fig. 2D. In both cases, [1-^{13}C]pyruvate arrived at about 20 s and reached a maximum at 24 s. [1-^{13}C]Lactate reached a maximum signal plateau at about 30 s after the end of injection.

For the patients who had unambiguous regions of tumor, the maximum SNRs of [1-^{13}C]pyruvate and [1-^{13}C]lactate in slices containing tumor were 101.3 (range, 31.6 to 192.1) and 19.5 (range, 12.5 to 33.5), respectively. Fitting the time course of changes in peak heights using a previously published two-compartment kinetic model (22) resulted in an estimated mean T_1 of [1-^{13}C]pyruvate and [1-^{13}C]lactate of 29.2 ± 5 s and 25.2 ± 5 s (SD), respectively, and a mean [1-^{13}C]pyruvate to [1-^{13}C]lactate conversion rate constant of 0.013 ± 0.003 s^{-1} (SD) (range, 0.009 to 0.016).

2D dynamic MRSI

A concern with the 1D localized dynamic MRSI data was that the contribution from hyperpolarized signals in tissues outside the prostate could confound the interpretation of estimated parameters. Therefore, five patients in phase 2 were studied with 2D spatially localized dynamic data. One of these patients had a PSA of 3.6 ng/ml and biopsy-proven prostate cancer in the left apex (Gleason grade 3 + 4) with an associated focus of reduced signal intensity on the anatomic images obtained during the MR staging examination (Fig. 3A). Hyperpolarized [1-^{13}C]pyruvate and [1-^{13}C]lactate from voxels in the prostate (Fig. 3B), the tumor (Fig. 3C), and a vessel outside the prostate (Fig. 3D) demonstrated a similar time course of delivery of the agent. There was increased conversion of [1-^{13}C]pyruvate to [1-^{13}C]lactate in the tumor (Fig. 3C), with the [1-^{13}C]pyruvate reaching a maximum by 18 ± 4 s and the [1-^{13}C]lactate reached a maximum at 27 ± 2 s after the start of acquisition, which was 5 s after the end of injection. After adjusting for additional delay, the timings of maximal signal are similar to those for the 1D dynamic data. Overall, the rate constant (mean ± SD) was 0.045 ± 0.025 s^{-1} for [1-^{13}C]pyruvate to [1-^{13}C]lactate in tumor voxels and 0.009 ± 0.003 s^{-1} for voxels coming from regions that included blood vessels.

Single–time point MRSI

The purpose of the single–time point spatially localized data was to compare the relative levels of [1-^{13}C]lactate and [1-^{13}C]pyruvate in regions of tumor versus normal prostate and surrounding tissue. For the phase 1 study, the MRSI acquisitions were initially started at about 30 s after the end of the injection. The maximum SNR for [1-^{13}C]pyruvate peaks in the prostate for the three patients evaluated in phase 1 with single–time point spatially localized MRSI doses of 0.14, 0.28, and 0.43 ml/kg were in the range of 4.5 to 8.4, 6.5 to 10.6, and 14.3 to 25.4, respectively. Hence, although [1-^{13}C]lactate peaks were observed in tumor voxels at the two lower doses, the higher levels of [1-^{13}C]pyruvate at 0.43 ml/kg allowed for a more reliable estimate of the ratio of [1-^{13}C]lactate/[1-^{13}C]pyruvate. In the following discussion on variations in this ratio in the prostate gland, we focus on the results from single–time point MRSI data that were obtained at the highest dose during phases 1 and 2 of the study.

Representative 2D MRSI data are shown in Fig. 4. The patient had a serum PSA of 9.5 ng/ml and bilateral biopsy-proven Gleason grade 3 + 3 prostate cancer. The T_2 images, apparent diffusion coefficient (ADC) images, and ^{1}H spectra from the staging examination demonstrated an abnormal lesion, but only on the right side of the gland (Fig. 4). The ^{13}C spectra were acquired from 33 to 45 s after the end of the injection, and the corresponding [1-^{13}C]lactate/[1-^{13}C]pyruvate image overlay, which highlights in color regions with a ratio of more than 0.6, demonstrated bilateral areas of hyperpolarized [1-^{13}C]lactate. The median [1-^{13}C]lactate/[1-^{13}C]pyruvate ratios were 0.94 (range, 0.85 to 1.25) on the right side and 1.35 (range, 0.73 to 4.39) on the left side of the gland. The median [1-^{13}C]lactate/[1-^{13}C]pyruvate ratio in a region of the central gland—which was not thought to include tumor—was 0.45 (range, 0.31 to 0.49). The median SNRs of [1-^{13}C]lactate in the right and left regions of suspected tumor were 7.6 and 6.7, with the corresponding median SNRs of [1-^{13}C]pyruvate being 7.8 and 5.4, respectively. MR-guided biopsy that was performed subsequent to the ^{13}C study confirmed the presence of bilateral cancer corresponding to these abnormalities, with Gleason grade 3 + 4 on the right and Gleason grade 3 + 3 with high-grade prostatic intraepithelial neoplasia on the left side of the gland. The fact that the hyperpolarized imaging method was able to detect bilateral cancer, whereas conventional anatomic imaging methods were only able to visualize unilateral cancer, is an exciting finding, which may be especially important in monitoring patients like this who are thought to have slow-growing cancers and are being followed with active surveillance before starting treatment.

One concern in interpreting the data from the patient in Fig. 4 was that the SNR of the [1-^{13}C]pyruvate peak was relatively low in some voxels, making it difficult to obtain an accurate estimate of the ratio of [1-^{13}C]lactate/[1-^{13}C]pyruvate for tumor versus normal tissue. For this reason, subsequent data sets were obtained starting at the earlier time of 25 s after the end of injection rather than at 33 s. For data acquired in this time window, peaks of [1-^{13}C]pyruvate were observed in most of the gland, and the criteria used to define regions of suspected tumor within the prostate gland were an SNR of [1-^{13}C]pyruvate >10.0, a clearly visualized peak corresponding to [1-^{13}C]lactate peak with an SNR >3.0, and the ratio of the peak heights of 0.2 or higher. An example of 3D localized ^{13}C MRSI data acquired

and evaluated in this manner is seen in Fig. 5. The results from the corresponding MR staging examination are shown in fig. S1. This patient (patient A in Table 2) had serum PSA of 4.5 ng/ml and a diagnosis of bilateral biopsy-proven Gleason grade 3 + 3 cancer. The ^{13}C spectral data showed large peaks corresponding to [1-^{13}C]pyruvate throughout the spectral grid with lower, but still clearly detected, [1-^{13}C]lactate peaks in the highlighted region. The median estimates for levels of [1-^{13}C]pyruvate, [1-^{13}C]lactate, and [1-^{13}C]lactate/ [1-^{13}C]pyruvate for tumor voxels identified on multiple slices as being tumor were 41.0, 13.6, and 0.28, respectively (Table 2). The color metabolite overlays highlight regions with [1-^{13}C]lactate/ [1-^{13}C]pyruvate that were higher than the cutoff value on multiple slices. The patient had a follow-up MR-guided biopsy that demonstrated that the lesion had progressed to Gleason 3 + 4 prostate cancer.

Results from three other patients who had areas of elevated [1-^{13}C]lactate/ [1-^{13}C]pyruvate are shown in Fig. 6 and Table 2. The same acquisition timing was used to obtain the MRSI data and the same cutoff criteria applied to define voxels with abnormal metabolite ratios as for patient A. For two of the cases (patients B and D), bilateral regions of suspected tumor were identified, and for the third case, there was a unilateral focus of suspected tumor. As can be seen in Table 2, the median ratios of [1-^{13}C]lactate/[1-^{13}C]pyruvate ranged from 0.28 to 0.38, the median SNR for [1-^{13}C]lactate ranged from 4.8 to 8.4, and the median SNR for [1-^{13}C]pyruvate ranged from 13.5 to 30.0. The locations highlighted in color on the metabolite overlay images were consistent either with the original biopsies from these patients or with abnormalities that were identified in the images from their MR staging examinations.

Discussion

First-in-man metabolic imaging with hyperpolarized [1-^{13}C]pyruvate was successfully applied in 31 patients with prostate cancer. There were no DLTs observed, and the highest dose, namely, 230 mM [1-^{13}C]pyruvate (0.43 ml/kg), was selected for evaluation of different MR data acquisition strategies in phase 2 of the study. The prototype polarizer and QC procedures used to prepare the hyperpolarized agent were complex, and the fact that 31 of 33 preparations were successful in producing material that was injected into the patients is encouraging. Future studies would benefit from the development of more robust and automated procedures for generating and preparing the hyperpolarized agent for human use. An improved system that can simultaneously polarize four samples and uses a disposable fluid path has been designed (23) and tested in preclinical studies (24). It is anticipated that clinical studies will take advantage of such technology to provide higher polarizations and faster agent delivery.

The kinetics of delivering the hyperpolarized agent and the increase in [1-^{13}C]lactate signal were consistent with those observed in preclinical models (25–29). The 1D dynamic MRSI data obtained in our study showed higher [1-^{13}C]lactate signal in slices including tumor, but also contained some signal from tissues outside of the prostate. The [1-^{13}C]lactate signal was low or undetectable in slices from regions of the prostate that did not include tumor. This agrees with previous patient prostate biopsy studies, which demonstrated very low lactate concentrations (30), and with preclinical studies, which demonstrated a low flux of

hyperpolarized [1-^{13}C]pyruvate to lactate in normal prostate (17). The 2D dynamic MRSI data were able to distinguish signals from tumor and vessels, with the rate of [1-^{13}C]pyruvate to [1-^{13}C]lactate conversion being four to five times higher in tumor. This is consistent with the increased expression of MCT1, MCT4, and LDH-A, and increased activity of LDH in the tumor that was observed in preclinical studies (17, 18).

The 2D and 3D single–time point MRSI data had excellent SNRs and spectral quality. These data sets were acquired in 8 to 12 s and accurately reflected the presence, location, and size of cancer relative to surrounding healthy prostate tissues. Moving to the earlier spectral acquisition window of 25 s after injection, for the patients shown in Figs. 5 and 6, yielded higher hyperpolarized [1-^{13}C]pyruvate signals and more readily quantifiable [1-^{13}C]lactate/[1-^{13}C]pyruvate ratios (Table 2) than for the patient shown in Fig. 4. The marked changes in hyperpolarized [1-^{13}C]pyruvate signal with time and differences in kinetics suggest that the acquisition of spatially localized dynamic MR data is a promising approach for comparing metabolic parameters for tumor versus normal tissue.

Patients who participated in phase 2 of the study and who had regions of abnormal signal on their previous multiparametric MR screening examinations also had elevated [1-^{13}C]lactate/[1-^{13}C]pyruvate relative to signals from normal prostate. In Fig. 4, our hyperpolarized imaging method highlighted a region of biopsy-proven tumor that was not observed during the staging examination; this is important because it shows the power of using more advanced technologies for characterizing tissues that appear normal on conventional anatomic images. There were two other subjects with findings of abnormal [1-^{13}C]lactate/[1-^{13}C]pyruvate in regions where the anatomic imaging was uncertain, but in those cases, no direct biopsy evidence was available to confirm that they corresponded to tumor.

There are several limitations of our study because it is first in human. Although ^{13}C data acquisition parameters had been investigated in phantom and preclinical studies, it was not possible to choose the most appropriate values without having results from human subjects. This led to adjustments in the timing parameters and spatial resolution being made during the course of the study. Although this did not influence the goals of phase 1 of the study, which were to establish the safety and feasibility of using hyperpolarized [1-^{13}C]pyruvate in humans, it did mean that the more detailed analysis of data was restricted to subjects participating in phase 2. Another limitation was that the population chosen for the study had relatively early-stage cancer, and it was not always possible to make exact correlations between the imaging findings and pathologic findings. The choice of patients with early-stage disease who were on active surveillance was driven by the need to avoid complications in data interpretation associated with previous treatment and to have plenty of time to recruit and monitor them during a period when they were expected to have stable disease. Evidence from preclinical studies has shown that the magnitude of [1-^{13}C]lactate/[1-^{13}C]pyruvate increases with tumor grade (18), and so we believe that our technology will be even more sensitive for evaluating patients with advanced and aggressive cancers.

When combined with findings from preclinical studies, the results of this first-in-man study suggest that hyperpolarized ^{13}C metabolic imaging may be valuable for initial diagnosis and

for monitoring therapy. In addition to improved technology for generating and delivering hyperpolarized agents becoming available (23), designing new MR data acquisition sequences that use compressed sensing (31), parallel imaging strategies, and multichannel ^{13}C radio frequency coils (32, 33) will help in translating these methods into the clinic. These developments will allow similar methods to be applied to more diverse populations of cancer patients who are undergoing surgical resection or image-directed biopsy. In addition to having the potential for more accurate diagnosis and staging, there have been a large number of studies using hyperpolarized agents in preclinical models of lymphoma (20), prostate (16–18), brain (26, 34), liver (25), breast (29), and bone cancers (19). Other disease models that have been studied and show promise for translation to humans are cardiac disease (33, 35, 36) and arthritis (37).

Materials and Methods

Patient population

Eligible patients were recruited from the prostate cancer clinic at University of California, San Francisco (UCSF), and had untreated, biopsyproven localized prostate cancer with no significant history of cardiac or pulmonary disease and adequate baseline organ function. They were required to have received a multiparametric ^{1}H MR staging examination before the hyperpolarized MR study to confirm that they had observable lesions and ensure that they were familiar with standard imaging procedures (Supplementary Methods). The process for generating the agent and the clinical protocol had received approval as an Investigational New Drug (IND) from the U.S. Food and Drug Administration. Patients provided written informed consent for participation in the imaging study.

Study design

The purpose of this study was to establish the safety and feasibility of using hyperpolarized metabolic imaging with [1-^{13}C]pyruvate in patients with prostate cancer. For phase 1 of the study, the commonly used 3 + 3 dose escalation clinical trial design was modified to enroll six patients at each dose: three to monitor the kinetics of delivery and three to evaluate the spatial distribution of metabolism in tumor versus other tissues. Three dose levels were considered (0.14, 0.28, or 0.43 ml/kg actual body weight of 230 mM pyruvate solution). Patients underwent continuous electrocardiogram monitoring during and for 10 min after the injection, as well as at baseline, 1 hour, and 2 hours after the injection. Clinical monitoring was undertaken for 2 hours after injection, with clinical and laboratory assessments performed at 24 hours and 7 days.

Toxicities were graded with CTCAE v4.0. criteria (21). A DLT was defined as an event of grade 2, 3, or 4 that was attributable to the agent and occurred within 7 days after the imaging examination. The stopping rule in each cohort of six subjects was as follows: if 0 or 1 dose DLT were observed, the study would proceed to the next dose level; if two DLTs were observed, that dose would become the maximum tolerated dose; and if more than two DLTs occur, the next lower dose would be considered as the maximum tolerated dose. Once either the maximum dose or the maximum tolerated dose cohorts were completed, phase 2

of the study design included an expansion cohort to optimize the imaging protocol and explore the biological variability in delivery, transport, and metabolism of the agent.

Formulation

The formulation comprised [1-^{13}C]pyruvate (22.0 mg/ml) (Supplementary Methods), sodium (4.1 mg/ml), tris (12.1 mg/ml), EDTA (0.1 mg/ml), and tris{8-carboxyl-2,2,6,6-tetra[2-(1-methoxyethyl)]benzo(1,2-d:4,5-d′)bis(1,3)dithiole-4-yl}methyl (radical) (4.6 mg/ml) in sterile water for injection. All components were manufactured according to current Good Manufacturing Practices and were provided in sterile single-use packaging by GE Healthcare.

^{13}C MR examination protocol

An intravenous catheter was placed, and the patient was positioned in a clinical 3-T MR scanner (GE Healthcare). For anatomic imaging, the ^{1}H body coil was used for transmission with a pelvic phased array and custom-designed ^{1}H/^{13}C endorectal coil for reception (Fig. 1). For ^{13}C data, a bore-insertable volume coil that was hinged like a clamshell to facilitate patient entry was used for transmission with the ^{13}C channel of the endorectal coil for reception (38). Anatomic images comprising a scout, sagittal, and axial T_2-weighted fast spin echo sequences were acquired first, followed by ^{13}C signal calibration that used the signal from a sealed standard housed within the endorectal coil containing 600 μl of 8 M ^{13}C-urea. Once the appropriate scan parameters had been defined, the operators in the clean room started the dissolution. If the sample satisfied the tests imposed by the QC system and the pharmacist who was monitoring the study gave their approval, the formulation was injected into the patient at ∼5 ml/s and ^{13}C data were obtained.

Acquisition parameters for ^{13}C MRSI data

Spatially localized dynamic ^{13}C spectroscopic imaging monitored delivery, transport, and metabolism of hyperpolarized [1-^{13}C]pyruvate. Single–time point 2D or 3D acquisitions were used to obtain arrays of ^{13}C spectra from the prostate and surrounding tissues in 8 to 12 s. The initial sequence parameters were chosen on the basis of studies in murine and dog models (16, 17, 22), but were further refined as the study progressed in terms of the start times for acquiring MR data and the flip angle schemes used (see below).

1D dynamic MRSI data—Spectra were obtained every 3 s starting at the end of the injection from a 36- to 60-mm axial slice encompassing the prostate. Echo planar localization was applied in the right-left direction at 10-mm resolution and with echo time (TE)/repetition time (TR)/flip angle of 2 ms/3 s/10°.

2D localized dynamic MRSI data—Spectra were obtained every 5 s starting at 5 s after the end of injection from a 12- to 40-mm axial slice with eight-phase encodes in one dimension and with 18-step echo planar localization in the other dimension to provide 10-mm in-plane resolution. The radio frequency pulses that were used applied either a 10° flip angle for all metabolites or a specially designed pulse that gave a flip angle of 10° for pyruvate and 20° for lactate. The TE/TR was 3/125 ms.

2D single–time point MRSI data—Spectra were obtained from a 10- to 20-mm axial slice with 12 by 12–phase encodes and 7-mm in-plane resolution with a progressive flip angle and TE/TR of 3/85 ms. The acquisition time was 12 s and started 25 to 33 s after the end of the injection. The variation in slice thickness was required to cover the region of putative tumor.

3D single–time point MRSI data—A 3D array of spectra was obtained from a 43- to 120-mm axial slice with 12 by 8 to 12–phase encodes and 18 echo planar frequency encodes. The in-plane resolution was 7 mm and the through-plane resolution was 7 to 15 mm, with a progressive flip angle and TE/TR of 3/85 to 125 ms. Variations of the in-plane slice thickness, number of phase encodes, and spatial resolution were driven by differences in the size of the prostate and the spatial extent of the region of tumor. The acquisition time was 8 to 12 s, and it started 25 to 33 s after the end of the injection.

Data analysis

The analysis of the ^{13}C MR data used specialized software developed in our laboratory (39). Arrays of spectra were obtained by apodizing the raw data with a 10-Hz Lorentzian function in the time domain and performing a Fourier transform. For data with echo planar localization, signals from the positive and negative gradient lobes were separately reconstructed for each trajectory with regridding of samples on the ramps. The spectral arrays were then zero- and first-order phase-corrected. Quantification of individual spectra used automatic phasing, baseline subtraction, and frequency correction. The heights and areas of spectral peaks were estimated and used to generate metabolite images and/or curves of the time course of changes in [1-^{13}C]lactate and [1-^{13}C]pyruvate.

The spectral arrays and metabolite images were directly correlated with anatomic images that were acquired within the same examination. For comparison purposes, regions of prostate cancer were identified as areas with concordant positive TRUS-guided biopsy and MRI abnormality within the same sextant of the prostate. Visual comparisons of the locations of regions with elevated lactate/pyruvate on the ^{13}C images were made with the results from the MR staging examination using anatomic images from the two studies as a reference to see whether similar regions were identified as having abnormalities. For voxels where the SNR of the dynamic data was sufficient, the curves of lactate and pyruvate were fit with the two-compartment model that was developed and applied in previous preclinical studies (22).

Supplementary Material

Refer to Web version on PubMed Central for supplementary material.

Acknowledgments

We acknowledge the important contributions to the success of the trial from M. McPolin, B. Jimenez, S. Hu, J. Crane, H. Yoshihara, C. Sotto, K. Grycz, and M. Contreras from UCSF; C. Cunningham from the University of Toronto; and P. Calderon, T. Skloss, P. Sontum, M. Thaning, G. Torheim, J. Wolber, Y.-F. Yen, and M. Mendizabal from GE Healthcare.

Funding: Pulse sequence and clinical study design were supported by NIH grants R01 EB007588 and R21 EB005363. The polarizer and costs of the ^{13}C patient studies were supported with funding from GE Healthcare.

References and Notes

1. Siegel R, Naishadham D, Jemal A. Cancer statistics, 2012. CA Cancer J Clin. 2012; 62:10–29. [PubMed: 22237781]
2. Han M, Partin AW, Piantadosi S, Epstein JI, Walsh PC. Era specific biochemical recurrence-free survival following radical prostatectomy for clinically localized prostate cancer. J Urol. 2001; 166:416–419. [PubMed: 11458039]
3. McNeal JE, Bostwick DG, Kindrachuk RA, Redwine EA, Freiha FS, Stamey TA. Patterns of progression in prostate cancer. Lancet. 1986; 1:60–63. [PubMed: 2867314]
4. Cooperberg MR, Carroll PR, Klotz L. Active surveillance for prostate cancer: Progress and promise. J Clin Oncol. 2011; 29:3669–3676. [PubMed: 21825257]
5. Wei JT, Dunn RL, Sandler HM, McLaughlin PW, Montie JE, Litwin MS, Nyquist L, Sanda MG. Comprehensive comparison of health-related quality of life after contemporary therapies for localized prostate cancer. J Clin Oncol. 2002; 20:557–566. [PubMed: 11786586]
6. Johansson JE, Andrén O, Andersson SO, Dickman PW, Holmberg L, Magnuson A, Adami HO. Natural history of early, localized prostate cancer. JAMA. 2004; 291:2713–2719. [PubMed: 15187052]
7. Bill-Axelson A, Holmberg L, Ruutu M, Häggman M, Andersson SO, Bratell S, Spångberg A, Busch C, Nordling S, Garmo H, Palmgren J, Adami HO, Norlén BJ, Johansson JE. Scandinavian Prostate Cancer Group Study No. 4, Radical prostatectomy versus watchful waiting in early prostate cancer. N Engl J Med. 2005; 352:1977–1984. [PubMed: 15888698]
8. Mehta SS, Lubeck DP, Sadetsky N, Pasta DJ, Carroll PR. Patterns of secondary cancer treatment for biochemical failure following radical prostatectomy: Data from CaPSURE. J Urol. 2004; 171:215–219. [PubMed: 14665879]
9. Kelloff GJ, Choyke P, Coffey DS. Prostate Cancer Imaging Working Group, Challenges in clinical prostate cancer: Role of imaging. AJR Am J Roentgenol. 2009; 192:1455–1470. [PubMed: 19457806]
10. Kurhanewicz J, Vigneron DB. Advances in MR spectroscopy of the prostate. Magn Reson Imaging Clin N Am. 2008; 16:697–710. [PubMed: 18926432]
11. Weinreb JC, Blume JD, Coakley FV, Wheeler TM, Cormack JB, Sotto CK, Cho H, Kawashima A, Tempany-Afdhal CM, Macura KJ, Rosen M, Gerst SR, Kurhanewicz J. Prostate cancer: Sextant localization at MR imaging and MR spectroscopic imaging before prostatectomy—Results of ACRIN prospective multi-institutional clinicopathologic study. Radiology. 2009; 251:122–133. [PubMed: 19332850]
12. Beauregard JM, Williams SG, Degrado TR, Roselt P, Hicks RJ. Pilot comparison of F-fluorocholine and F-fluorodeoxyglucose PET/CT with conventional imaging in prostate cancer. J Med Imaging Radiat Oncol. 2010; 54:325–332. [PubMed: 20718912]
13. Ardenkjaer-Larsen JH, Fridlund B, Gram A, Hansson G, Hansson L, Lerche MH, Servin R, Thaning M, Golman K. Increase in signal-to-noise ratio of > 10,000 times in liquid-state NMR. Proc Natl Acad Sci USA. 2003; 100:10158–10163. [PubMed: 12930897]
14. Golman K, in ‘t Zandt R, Thaning M. Real-time metabolic imaging. Proc Natl Acad Sci USA. 2006; 103:11270–11275. [PubMed: 16837573]
15. Golman K, Petersson JS. Metabolic imaging and other applications of hyperpolarized $^{13}C^{1}$. Acad Radiol. 2006; 13:932–942. [PubMed: 16843845]
16. Chen AP, Albers MJ, Cunningham CH, Kohler SJ, Yen YF, Hurd RE, Tropp J, Bok R, Pauly JM, Nelson SJ, Kurhanewicz J, Vigneron DB. Hyperpolarized C-13 spectroscopic imaging of the TRAMP mouse at 3T—Initial experience. Magn Reson Med. 2007; 58:1099–1106. [PubMed: 17969006]
17. Keshari KR, Sriram R, Van Criekinge M, Wilson DM, Wang ZJ, Vigneron DB, Peehl DM, Kurhanewicz J. Metabolic reprogramming and validation of hyperpolarized ^{13}C lactate as a

prostate cancer biomarker using a human prostate tissue slice culture bioreactor. Prostate. 2013; 73:1171–1181. [PubMed: 23532911]

18. Albers MJ, Bok R, Chen AP, Cunningham CH, Zierhut ML, Zhang VY, Kohler SJ, Tropp J, Hurd RE, Yen YF, Nelson SJ, Vigneron DB, Kurhanewicz J. Hyperpolarized ^{13}C lactate, pyruvate, and alanine: Noninvasive biomarkers for prostate cancer detection and grading. Cancer Res. 2008; 68:8607–8615. [PubMed: 18922937]
19. Dafni H, Larson PE, Hu S, Yoshihara HA, Ward CS, Venkatesh HS, Wang C, Zhang X, Vigneron DB, Ronen SM. Hyperpolarized ^{13}C spectroscopic imaging informs on hypoxia-inducible factor-1 and myc activity downstream of platelet-derived growth factor receptor. Cancer Res. 2010; 70:7400–7410. [PubMed: 20858719]
20. Day SE, Kettunen MI, Gallagher FA, Hu DE, Lerche M, Wolber J, Golman K, Ardenkjaer-Larsen JH, Brindle KM. Detecting tumor response to treatment using hyperpolarized ^{13}C magnetic resonance imaging and spectroscopy. Nat Med. 2007; 13:1382–1387. [PubMed: 17965722]
21. National Cancer Institute. Common Terminology Criteria for Adverse Events (CTCAE) v4.0. http://ctep.cancer.gov
22. Zierhut ML, Yen YF, Chen AP, Bok R, Albers MJ, Zhang V, Tropp J, Park I, Vigneron DB, Kurhanewicz J, Hurd RE, Nelson SJ. Kinetic modeling of hyperpolarized $^{13}C_1$-pyruvate metabolism in normal rats and TRAMP mice. J Magn Reson. 2010; 202:85–92. [PubMed: 19884027]
23. Ardenkjaer-Larsen JH, Leach AM, Clarke N, Urbahn J, Anderson D, Skloss TW. Dynamic nuclear polarization polarizer for sterile use intent. NMR Biomed. 2011; 24:927–932. [PubMed: 21416540]
24. Hu S, Larson PE, Vancriekinge M, Leach AM, Park I, Leon C, Zhou J, Shin PJ, Reed G, Keselman P, von Morze C, Yoshihara H, Bok RA, Nelson SJ, Kurhanewicz J, Vigneron DB. Rapid sequential injections of hyperpolarized [1-^{13}C]pyruvate in vivo using a sub-kelvin, multi-sample DNP polarizer. Magn Reson Imaging. 2013; 31:490–496. [PubMed: 23107275]
25. Hu S, Balakrishnan A, Bok RA, Anderton B, Larson PE, Nelson SJ, Kurhanewicz J, Vigneron DB, Goga A. ^{13}C-pyruvate imaging reveals alterations in glycolysis that precede c-Myc-induced tumor formation and regression. Cell Metab. 2011; 14:131–142. [PubMed: 21723511]
26. Park I, Bok R, Ozawa T, Phillips JJ, James CD, Vigneron DB, Ronen SM, Nelson SJ. Detection of early response to temozolomide treatment in brain tumors using hyperpolarized ^{13}C MR metabolic imaging. J Magn Reson Imaging. 2011; 33:1284–1290. [PubMed: 21590996]
27. Pullinger B, Profka H, Ardenkjaer-Larsen JH, Kuzma NN, Kadlecek S, Rizi RR. Metabolism of hyperpolarized [1-^{13}C]pyruvate in the isolated perfused rat lung—An ischemia study. NMR Biomed. 2012; 25:1113–1118. [PubMed: 22311307]
28. Ward CS, Venkatesh HS, Chaumeil MM, Brandes AH, Vancriekinge M, Dafni H, Sukumar S, Nelson SJ, Vigneron DB, Kurhanewicz J, James CD, Haas-Kogan DA, Ronen SM. Noninvasive detection of target modulation following phosphatidylinositol 3-kinase inhibition using hyperpolarized ^{13}C magnetic resonance spectroscopy. Cancer Res. 2010; 70:1296–1305. [PubMed: 20145128]
29. Witney TH, Kettunen MI, Hu DE, Gallagher FA, Bohndiek SE, Napolitano R, Brindle KM. Detecting treatment response in a model of human breast adenocarcinoma using hyperpolarised [1-^{13}C]pyruvate and [1,4-$^{13}C_2$]fumarate. Br J Cancer. 2010; 103:1400–1406. [PubMed: 20924379]
30. Tessem MB, Swanson MG, Keshari KR, Albers MJ, Joun D, Tabatabai ZL, Simko JP, Shinohara K, Nelson SJ, Vigneron DB, Gribbestad IS, Kurhanewicz J. Evaluation of lactate and alanine as metabolic biomarkers of prostate cancer using ^{1}H HR-MAS spectroscopy of biopsy tissues. Magn Reson Med. 2008; 60:510–516. [PubMed: 18727052]
31. Larson PE, Hu S, Lustig M, Kerr AB, Nelson SJ, Kurhanewicz J, Pauly JM, Vigneron DB. Fast dynamic 3D MR spectroscopic imaging with compressed sensing and multiband excitation pulses for hyperpolarized ^{13}C studies. Magn Reson Med. 2012; 65:610–619. [PubMed: 20939089]
32. Arunachalam A, Whitt D, Fish K, Giaquinto R, Piel J, Watkins R, Hancu I. Accelerated spectroscopic imaging of hyperpolarized C-13 pyruvate using SENSE parallel imaging. NMR Biomed. 2009; 22:867–873. [PubMed: 19489035]

33. Lau AZ, Chen AP, Ghugre NR, Ramanan V, Lam WW, Connelly KA, Wright GA, Cunningham CH. Rapid multislice imaging of hyperpolarized ^{13}C pyruvate and bicarbonate in the heart. Magn Reson Med. 2010; 64:1323–1331. [PubMed: 20574989]
34. Marjańska M, Iltis I, Shestov AA, Deelchand DK, Nelson C, Uğurbil K, Henry PG. In vivo ^{13}C spectroscopy in the rat brain using hyperpolarized [1-^{13}C]pyruvate and [2-^{13}C]pyruvate. J Magn Reson. 2010; 206:210–218. [PubMed: 20685141]
35. Moreno KX, Sabelhaus SM, Merritt ME, Sherry AD, Malloy CR. Competition of pyruvate with physiological substrates for oxidation by the heart: Implications for studies with hyperpolarized [1-^{13}C]pyruvate. Am. J Physiol Heart Circ Physiol. 2010; 298:H1556–H1564.
36. Schroeder MA, Cochlin LE, Heather LC, Clarke K, Radda GK, Tyler DJ. In vivo assessment of pyruvate dehydrogenase flux in the heart using hyperpolarized carbon-13 magnetic resonance. Proc Natl Acad Sci USA. 2008; 105:12051–12056. [PubMed: 18689683]
37. MacKenzie JD, Yen YF, Mayer D, Tropp JS, Hurd RE, Spielman DM. Detection of inflammatory arthritis by using hyperpolarized ^{13}C-pyruvate with MR imaging and spectroscopy. Radiology. 2011; 259:414–420. [PubMed: 21406626]
38. Tropp, J.; Calderon, P.; Vigneron, D. Systems, methods and apparatus for an endo-rectal receive-only probe. US Patent 7945308. 2011.
39. Crane JC, Olson MP, Nelson SJ. SIVIC: An open-source DICOM software framework and plug-in for OsiriX PACS, International Society for Magnetic Resonance in Medicine 18th Scientific Meeting. 2010

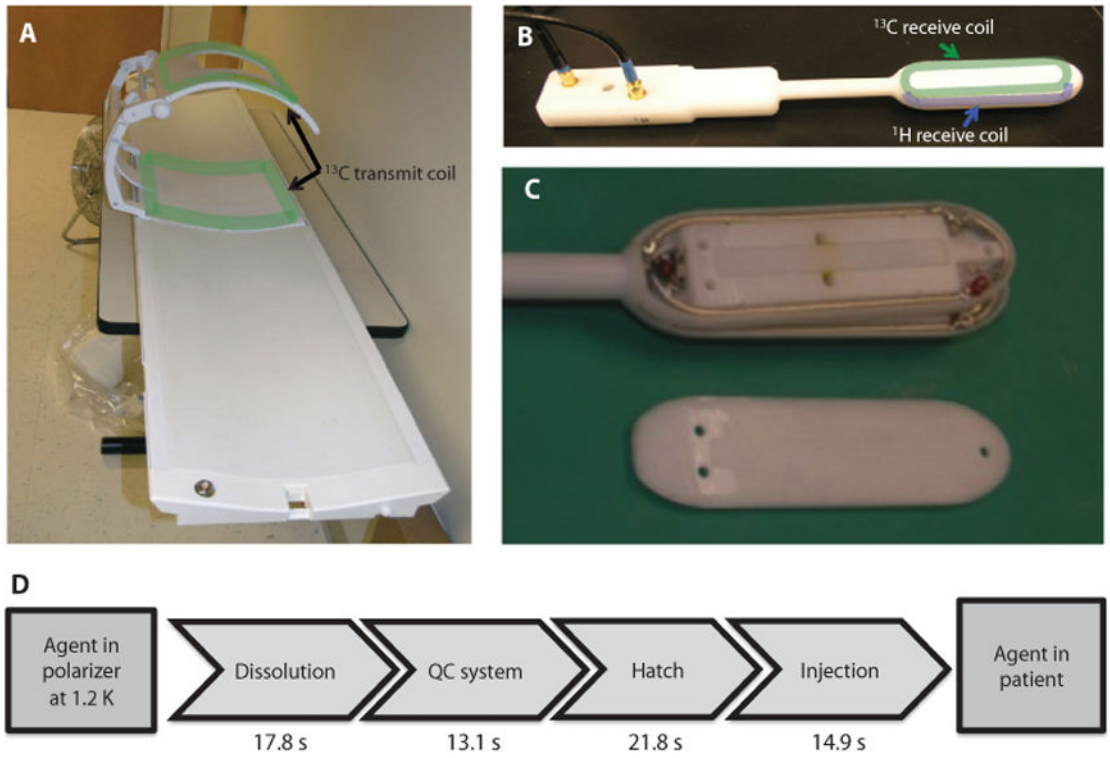

Fig. 1. ^{13}C coil setup and the schematic steps for the delivery of hyperpolarized [1-^{13}C]pyruvate

(**A** to **C**) ^{13}C transmit coil (A) and endorectal ^{1}H/^{13}C receiver coil (B) used for acquiring data. The location of the coils is outlined on (A) and (B), with the layers inside the endorectal coil being seen in (C). The dimensions of the elements in the endorectal coil were 4 inches × 1 inches, with the total length of the coil being 12 inches. (**D**) Steps involved in transferring the hyperpolarized agent from the polarizer to the patient, and mean times required for each of them.

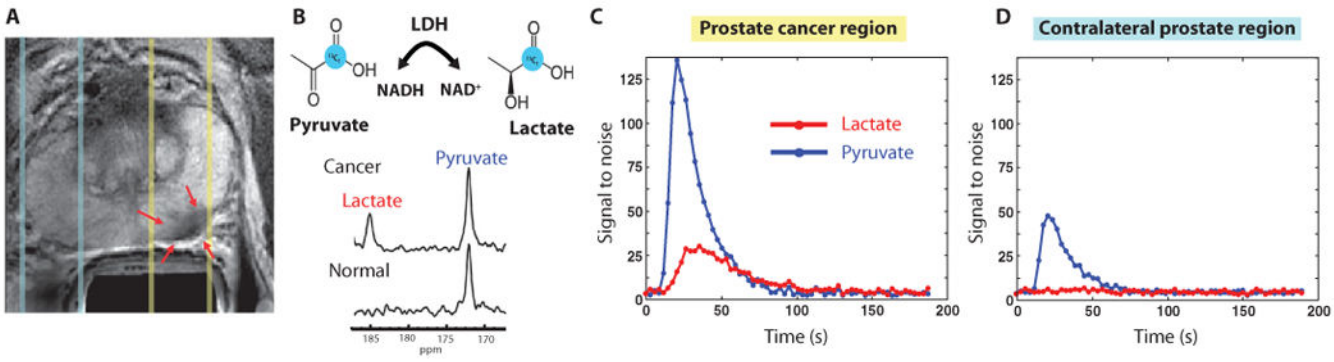

Fig. 2. 1D ^{13}C dynamic MRSI data

Images are from a representative patient with a current PSA of 12.2 ng/ml, a small volume of biopsy-proven Gleason grade 4 + 3 prostate cancer in the left midgland, and who received the lowest dose (0.14 ml/kg) of hyperpolarized [1-^{13}C]pyruvate. (**A**) Axial T_2-weighted image showing slices (dashed lines) obtained from 1D spectral localization. The slice that overlaps the left prostatic peripheral zone (right side of image) contained a small focus of reduced T_2 signal intensity corresponding to the region of biopsy-proven cancer (red arrows). The slice overlapping the right peripheral zone (left side of image) contains only normal prostate tissue. (**B**) Flux of [1-^{13}C]pyruvate to [1-^{13}C]lactate catalyzed by LDH (top). Dynamic ^{13}C spectra were obtained from the same patient in (A) at 36 s after injection of hyperpolarized [1-^{13}C]pyruvate (bottom). The cancer spectrum demonstrated a lactate SNR of 25 owing to a high flux of hyperpolarized [1-^{13}C]pyruvate to [1-^{13}C]lactate. (**C**) Plot of 1D localized dynamic hyperpolarized pyruvate and lactate data from the slice that overlapped the region of prostate cancer. (**D**) Plot of 1D localized dynamic hyperpolarized pyruvate and lactate data from the slice that overlapped a contralateral region of the prostate.

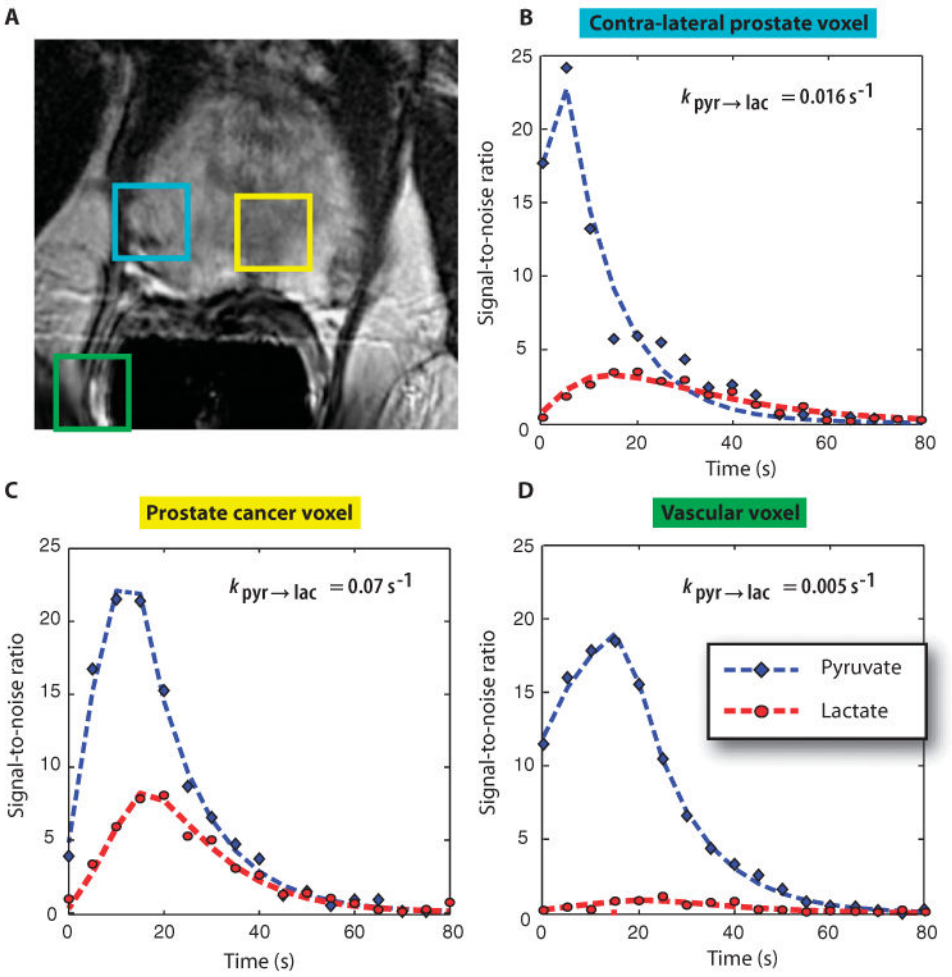

Fig. 3. 2D ^{13}C dynamic MRSI data

Images are from a representative patient with a current PSA of 3.6 ng/ml, who had biopsy-proven prostate cancer in the left apex (Gleason grade 3 + 4) and received the highest dose of hyperpolarized [1-^{13}C]pyruvate (0.43 ml/kg). (**A**) A focus of mild hypointensity can be seen on the T_2-weighted image, which was consistent with the biopsy findings. (**B** to **D**) 2D localized dynamic hyperpolarized [1-^{13}C]pyruvate and [1-^{13}C]lactate from spectral data that were acquired every 5 s from voxels overlapping the contralateral region of prostate (turquoise), a region of prostate cancer (yellow), and a vessel outside the prostate (green). The dynamic data were fit as described previously (22).

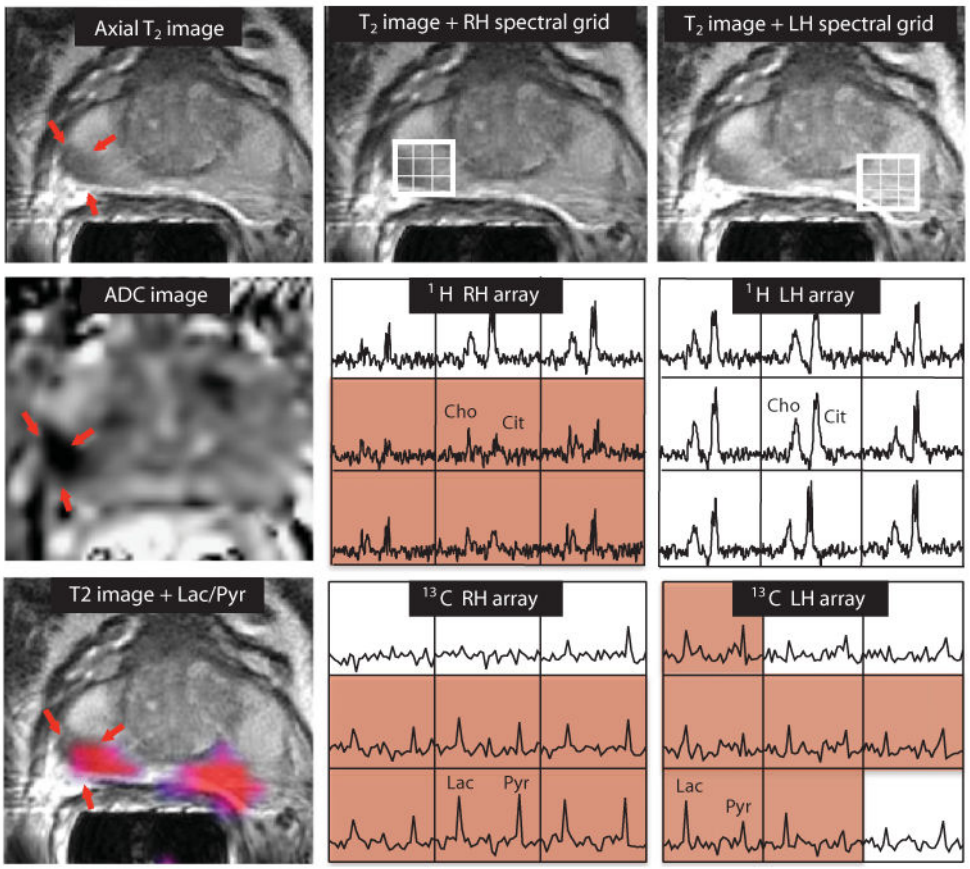

Fig. 4. 2D single–time point MRSI data

Images were obtained from a patient with serum PSA of 9.5 ng/ml, who was diagnosed with bilateral biopsy-proven Gleason grade 3 + 3 prostate cancer and received the highest dose of hyperpolarized [1-^{13}C]pyruvate (0.43 ml/kg). The axial T_2-weighted image shows a unilateral region of reduced signal intensity (red arrows), which is consistent with a reduction in the corresponding ADC. The ^{1}H spectral arrays supported these findings, with voxels with reduced citrate and elevated choline/citrate (highlighted in pink) on the right side of the gland and voxels with normal metabolite ratios on the left side. The ^{13}C spectral arrays show voxels with elevated levels of hyperpolarized [1-^{13}C]lactate/[1-^{13}C]pyruvate (highlighted in pink) on both the right and left sides of the prostate. The location of colored regions in the metabolite image overlay had a ratio of [1-^{13}C]lactate/[1-^{13}C]pyruvate greater than or equal to 0.6.

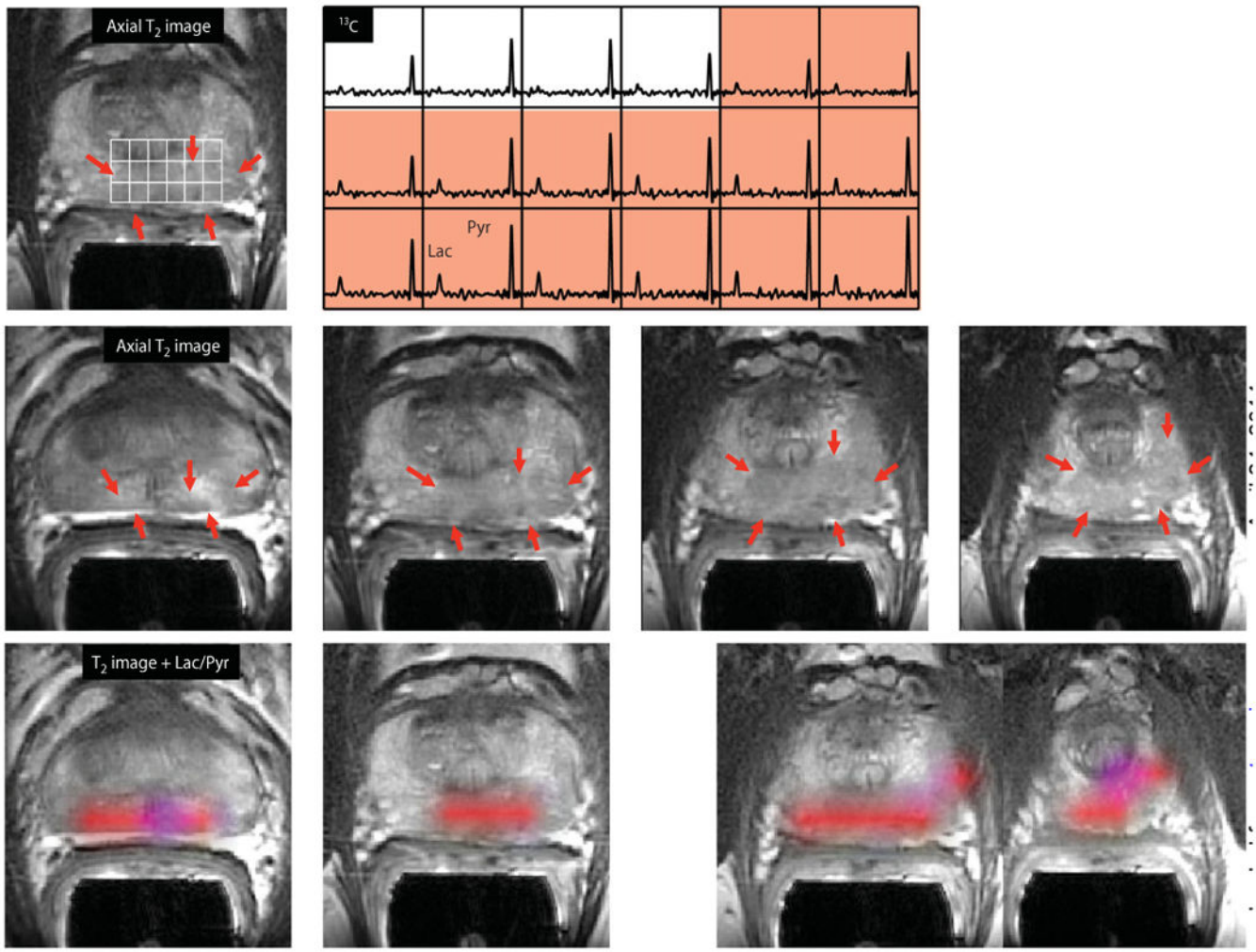

Fig. 5. 3D single–time point localized MRSI data

Images were obtained from patient A in Table 2, who had a serum PSA of 4.5 ng/ml, was originally diagnosed with bilateral biopsy-proven Gleason grade 3 + 3 prostate cancer, and received the highest dose of hyperpolarized [1-^{13}C]pyruvate (0.43 ml/kg). The upper panel shows an axial T_2-weighted images and corresponding spectral array with the area of putative tumor highlighted by pink shading. A region of tumor was observed on the T_2-weighted images (red arrows), as well as on ADC images and ^{1}H MRSI data (fig. S1). A region of relatively high hyperpolarized [1-^{13}C]lactate was observed in the same location as the abnormalities that had been observed on the multiparametric ^{1}H staging exam. The lower panels show axial T_2 images with and without metabolite overlays for different axial slices from the same patient. The colored regions in these overlays have a ratio of [1-^{13}C]lactate/[1-^{13}C]pyruvate ≥0.2. These demonstrated a large volume of bilateral cancer.

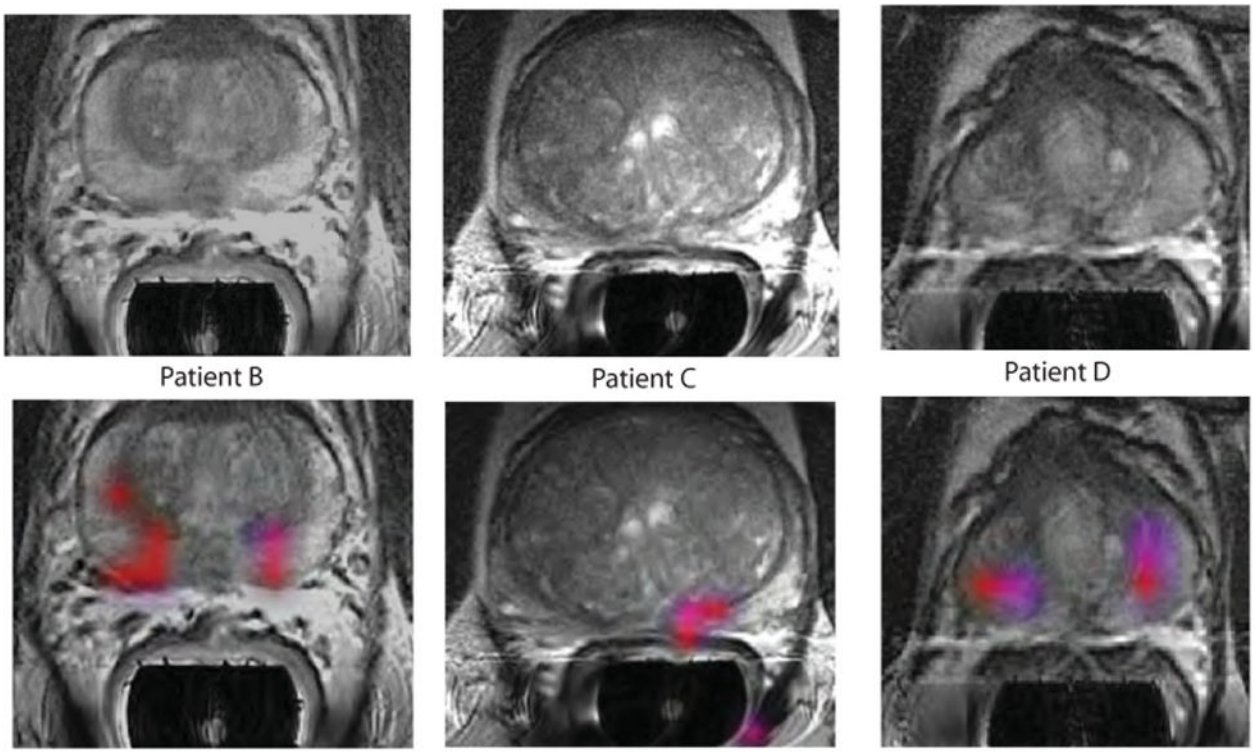

Fig. 6. Further representative examples of 3D single–time point MRSI data

The axial T_2-weighted images and overlays of hyperpolarized [1-^{13}C]lactate/[1-^{13}C]pyruvate are from the three patients labeled as B to D in Table 2. All three of the patients had biopsy-proven Gleason grade 3 + 3 prostate cancer and received the highest dose of hyperpolarized [1-^{13}C]pyruvate (0.43 ml/kg). Patient B had a current PSA of 5.1 ng/ml, patient C had a PSA of 9.8 ng/ml, and patient D had a PSA of 1.9 ng/ml. The SNR and metabolite ratios in the regions highlighted in color on the image overlays are given in Table 2.

Table 1

Summary of study design

Number of patients, doses of hyperpolarized [1-^{13}C]pyruvate given, and types of MR examinations performed in each component of the study are provided.

Study component	Dose (ml/kg)	*n* patients	Type of MR acquisition
Phase 1: Dose escalation	0.14	3	1D dynamic MRSI
		3	3D MRSI
	0.28	3	1D dynamic MRSI
		3	3D MRSI
	0.43	3	1D dynamic MRSI
		3	2D MRSI
Phase 2: Refining MR methods	0.43	5	2D dynamic MRSI
		3	2D MRSI
		5	3D MRSI

Table 2
Estimates of metabolite parameters within regions of tumor

The values shown are the median (range) of the SNR for hyperpolarized [1-^{13}C]lactate, hyperpolarized [1-^{13}C]pyruvate, and the ratios of these metabolites in tumor voxels for the patients shown in Figs. 5 and 6.

Subject	*n* voxels	[1-^{13}C]Lactate/[1-^{13}C]pyruvate	[1-^{13}C]Lactate SNR	[1-^{13}C]Pyruvate SNR
Patient A	11	0.28 (0.26–0.36)	13.6 (5.9–18.6)	41.0 (17.5–54.0)
Patient B	6	0.38 (0.32–0.47)	4.8 (3.6–7.8)	13.5 (10.1–20.0)
Patient C	3	0.32 (0.27–0.33)	6.3 (4.1–7.3)	22.5 (12.8–23.0)
Patient D	4	0.28 (0.24–0.33)	8.4 (6.4–16.1)	30.0 (27.8–49.4)